Acta Metall. Sin. (Engl. Lett.)
DOI 10.1007/s40195-014-0060-4

Structural Features of (Ce, La or Sr)(Mn or Co)O_3 Nano-Perovskites as a Catalyst for Carbon Monoxide Oxidation

Mahnaz Ghiasi · Azim Malekzadeh

Received: 7 May 2013 / Revised: 20 November 2013

Abstract The collection of different cations in the *A* and *B* sites of ABO_3 was explored for the regularity of perovskites phase formability. Here, Sr^{2+}, La^{3+}, and Ce^{4+} are selected as the cations of site *A*. The site *B* is considered to be Mn or Co cations. XRD analysis and Fourier transform infrared spectroscopy results confirm the formation of perovskite structure for catalysts in which La^{3+} and Sr^{2+} are considered as the cations of site *A*. Ceria is detected as the main crystalline phase when Ce^{4+} is selected to be cation of site *A*. It is found that the octahedral factor (r_B/r_O) takes the same important role as the tolerance factor to form cubic perovskite. Average crystallite size of the products was calculated by data of the XRD and measured by the TEM analysis. Results of the XRD and TEM studies were supported by the study of the particles size distribution, which was carried out in a particle size analyzer. The perovskite samples were also used for stoichiometric oxidation of carbon monoxide with air.

KEY WORDS: Carbon monoxide; Nano-perovskite; Oxidation; Cerium; Lanthanum; Strontium

1 Introduction

Carbon monoxide is an air pollutant emitted by many sources. Total oxidation of carbon monoxide to carbon dioxide is employed to meet environmental regulations in an economic way. Low temperature CO oxidation catalysts are used in residential and automotive air cleaning technologies, gas masks for mining applications, CO detectors, and selective oxidation of CO in reformer gas for fuel cell applications [1]. Precious metals (Pt, Pd) are well-known oxidation catalysts with high activity and stability, and are widely used for exhaust gas emission control [2]. However, due to the high cost of precious metals, recently more attention has been given to the use of none-noble metal catalysts. Perovskite-type mixed oxides (ABO_3), especially cubic structures, have shown promising results with many practical applications owing to their excellent physical and chemical properties [1]. The catalytic properties of perovskite-type oxides basically depend on the nature of *A* and *B* ions and on their valence state [3]. The *A* site ions are catalytically inactive. The nature of these ions, however, influences the stability of the perovskite phase. Catalytic activity is generally determined by the *B* cation [4].

Several synthesis methods for preparation of perovskite phases have been proposed and developed over the years. These methods include pyrolysis, co-precipitation, citrate complexation, spray-drying, freeze-drying, micro emulsion, and sol–gel process [5–7]. Combustion synthesis is an easy and convenient method for preparation of a variety of nano-materials [8]. In this technique, a thermally induced redox reaction takes place between an oxidant and a fuel. Many types of combustion synthesis exist which differ mainly in the physical state of the reactants or in the combustion modality. Citrate–nitrate auto-combustion synthesis (CNA) is a very popular solution combustion

Available online at http://link.springer.com/journal/40195

M. Ghiasi · A. Malekzadeh (✉)
School of Chemistry, Damghan University,
36715-364 Damghan, Iran
e-mail: malekzadeh@du.ac.ir

Published online: 05 May 2014

method, where the fuel is citric acid and metal nitrates are used as metal and oxidant source and can be more properly described as a sol–gel combustion method [9].

It is well documented that (La or Sr)BO_3 perovskites with Mn, Co, Fe, Ni, or Cr as cation of site *B* are efficient catalysts for CO oxidation [4, 6]. Ceria is known to be a proper oxygen activator with high oxygen storage capacity. Similar properties of Ce cation with La and Sr cations, such as atomic radius and coordination number, were our mainspring to have an effort for preparation of (Sr, La, or Ce)(Mn or CO)O_3 perovskites to compare their catalytic properties for carbon monoxide oxidation. The CNA method by the aim of obtaining nano-perovskite mixed oxides has been used.

2 Experimental

Samples of (Ce, La, or Sr)(Mn or Co)O_3 were prepared by the citrate–nitrate auto-combustion method using metal nitrate precursors in the presence of citric acid according to Table 1 and similar to the recipe reported elsewhere [1, 10]. To prepare catalysts, solutions with appropriate concentrations of metal nitrate and citric acid were mixed (total volume of 20 mL). The solutions were evaporated at 60 °C overnight. Thus, the obtained uniform and viscous materials were subsequently dried at 80 and 150 °C overnight, respectively. The resulting spongy and friable materials were completely powdered after each drying. The sequential dryings and powdering are carried out to obtain a more uniform sample for calcination. The final powders were calcined at 600 °C for 5 h. Samples were completely powdered and were subsequently calcined at 900 and 1,100 °C for 5 h.

The FTIR spectra of samples were recorded in a PERKIN-ELMER FTIR spectrometer in the wavenumber range of 450–1,850 cm^{-1}. X-ray diffraction patterns of the samples were recorded in the range of $2\theta = 10°$–$90°$ in a Bruker AXS diffractometer D8 ADVANCE with CuK_α radiation filtered by a nickel monochromator and operated at 40 kV and 30 mA. The morphology of the samples was studied by the SEM (Philips XL30) analysis. The particle size of the samples was investigated by the TEM (LEO Model 912AB) analysis. Particles size distribution of the samples was studied by a particle size analyzer (Cordouan Technologies Model VASCO). The surface area, pore volume and pore size diameter of the samples was measured by the BET method (Quantachrome NOVA 2000 USA). Catalytic CO oxidation tests were studied in an experimental setup using a quartz tube, filled with 200 mg of 60–100 mesh sized catalyst supported on ceramic wool under GHSV of 12,000 h^{-1}. In a typical experiment, a mixture of 6 vol% CO in Ar and air, a stoichiometric ratio with respect to oxygen, was passed through the catalyst bed with a total gas mixture flow rate of 40 mL/min at STP. Catalytic test studies were carried out by temperature rising in randomly intervals from 50 °C to complete oxidation temperature. The product stream was analyzed by a GC on a FI detector equipped with a methanizer. No carbon dioxide was detected using an empty reactor equipped with the ceramic wool.

3 Results and Discussion

Figure 1 displays the XRD patterns of the samples that are reported in Table 1. All diffraction peaks of X-ray match well with that of the reported X-pert high score PDF code:

Table 1 Experimental conditions for preparation of the samples, concentration of citric acid is 1 mol/L

Sample	Composition	Temperature of calcination (°C)	Concentration of $Mn(NO_3)_2{\cdot}4H_2O$ (mol/L)	Concentration of $Co(NO_3)_2{\cdot}6H_2O$ (mol/L)	Concentration of $Sr(NO_3)_2$ (mol/L)	Concentration of $La(NO_3)_3{\cdot}6H_2O$ (mol/L)	Concentration of $Ce(NO_3)_3{\cdot}6H_2O$ (mol/L)
No. 1	$LaCoO_3$	600	–	0.20	–	0.20	–
No. 2	$LaCoO_3$	900	–	0.20	–	0.20	–
No. 3	$LaMnO_3$	600	0.20	–	–	0.20	–
No. 4	$LaMnO_3$	900	0.20	–	–	0.20	–
No. 5	$SrCoO_3$	900	–	0.25	0.25	–	–
No. 6	$SrMnO_3$	900	0.25	–	0.25	–	–
No. 7	$CeCoO_3$	900	–	0.25	–	–	0.25
No. 8	$CeMnO_3$	900	0.20	–	–	–	0.20
No. 9	$CeMnO_3$	1100	0.20	–	–	–	0.20
No. 10[a]	$CeMnO_3$	1100	0.20	–	–	–	0.20

[a] Calcined at 1,100 °C under reductant atmosphere (6 vol% CO in Ar with flow rate of 5 mL/min)

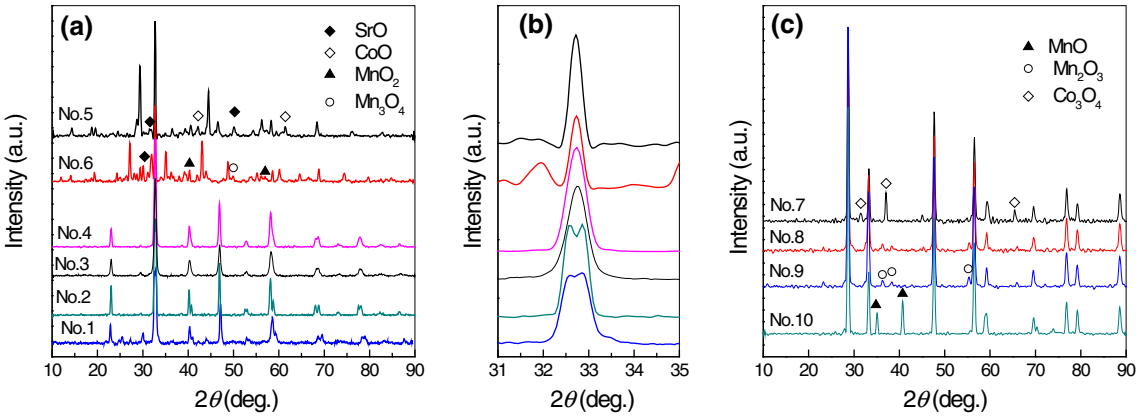

Fig. 1 XRD patterns of the synthesized samples Nos. 1–6 **a**, magnified graph of **a** in the 2θ range of 31°–35° **b** and XRD patterns of the synthesized samples Nos. 7–10 **c**, unmarked peaks in **a**, **c** are related to the perovskite and CeO_2 phases, respectively

01-086-1663 (Nos. 1 and 2), 01-075-0440 (Nos. 3 and 4), 00-048-0875 (No. 5), 00-024-1213 (No. 6), and 01-075-0076 (Nos. 7–10). Results of XRD analysis show that $LaMnO_3$ and $LaCoO_3$ are the phases that crystallize in the perovskite form during calcining at 600 °C, i.e., samples in which the La is considered as the cation of site *A* (samples Nos. 1 and 3 in Fig. 1a). Metal oxide crystalline phases, however, are detected for the rest of samples during calcining at 600 °C (data not shown). The perovskites of $SrMnO_3$ and $SrCoO_3$ are formed at a calcination temperature as high as 900 °C (samples Nos. 5 and 6 in Fig. 1a). Most prominent peak of perovskite at $\sim 33°$ is only observed for the samples in which strontium and lanthanum cations are considered as the cations of site *A*, after calcining at 900 °C. Results show that the La(Mn or Co)O_3 and Sr(Mn or Co)O_3 perovskites are formed while the Ce(Mn or Co)O_3 perovskites are not obtained during 5-h calcining at 600 and 900 °C. Instead of, CeO_2 is detected as the main crystalline phase (samples Nos. 7 and 8 in Fig. 1b). It is known that the normal valences of the La ions are 3+; however, Ce^{3+} ion is more easily oxidized to Ce^{4+} ion than the other trivalent lanthanide ions [11]. Results totally confirmed the influence of the cation of site A in the stability of the perovskite phase.

Crystallographic parameters of the prepared samples are summarized in Table 2. The interesting result of the study can be related to the formation of cubic structure of $LaMnO_3$ perovskite on preparation (samples Nos. 3, 4 in Fig. 1a and Table 2), for which few reports are available [1, 12, 13]. A hexagonal perovskite was detected as crystalline form of $SrMnO_3$ and $SrCoO_3$ catalysts (samples Nos. 5, 6 in Fig. 1a and Table 2). Small splitting of the main peak of the perovskite at $2\theta = 33°$ is an indicator of a rhombohedral system and is observed in the XRD pattern of $LaCoO_3$ samples (samples Nos. 1 and 2 in Fig. 1a).

The XRD data were also used to calculate the crystallite size of the samples (Table 3). A simple relationship between crystallite size *D* and peak broadening is offered by Scherrer equation [14, 15]:

$$D = \frac{K\lambda}{\beta\cos\theta}, \tag{1}$$

where *K* is known as Scherrer constant whose value is approximately 0.9, λ is the wavelength of X-ray, θ is the Bragg angle in radians and β is the width, in radians, of the peak due to size effects and was defined as the width at half maximum of the peak (FWHM). For an X-ray profile, β is calculated as $\beta = (\beta_{obs} - \beta_s)$, where β_{obs} is the width at half maximum measured for the specimen and β_s is the width at half maximum of an standard sample, defined as width due to instrument. Contribution of strain to the diffraction line broadening, however, is not negligible. The effect of the size and strain on peak broadening has been separated and developed by Williamson and Hall [16]. It is now known as the Williamson–Hall plot. The Williamson–Hall equation is expressed as:

$$\beta\cos\theta = \frac{K\lambda}{D} + 2\varepsilon\sin\theta, \tag{2}$$

where ε is the lattice strain. In this equation the width β, in radians, of the peak is due to the size and strain effects, i.e., $\beta = \beta_{size+strain}$ and is calculated as Scherrer equation. A linear extrapolation to the plot of $\beta\cos\theta$ against $2\sin\theta$ gives the particle size in form of ($K\lambda/D$) and the slope gives the strain ε.

Detected phases are observed to be in nano-sized scale (see Table 3). The crystallite sizes that are estimated from the XRD line profile by Williamson–Hall equation are larger than the ones calculated by the Scherrer formula. It is related to the some strain in these structures.

Results of XRD studies show that Ce(Mn or Co)O_3 perovskites are not formed upon calcining at 900 °C. The effect of Ce-doping of the site *A* has been reported; however, a perovskite with cerium as the only cation of site *A*

Table 2 Crystallographic parameters of the prepared nanoparticles

Sample	Composition	Crystal system	Space group	*a* (nm)	*c* (nm)	α (°)
Nos. 1 and 2	$LaCoO_3$	Rhombohedral	*R*-3	0.54	0.54	60
Nos. 3 and 4	$LaMnO_3$	Cubic	*Pm*-3*m*	0.39	0.39	90
No. 5	$SrCoO_3$	Hexagonal	–	0.55	0.42	90
No. 6	$SrMnO_3$	Hexagonal	*P*63/*mmc*	0.55	0.91	90
Nos. 7–10	CeO_2	Cubic	*Fm*-3*m*	0.54	0.54	90

Table 3 Crystallite size, BET, pore volume and pore diameter of the synthesized samples

Sample	Composition	Crystallite size (nm)		BET (m^2/g)	Total pore volume (mL/g)	Average pore diameter (nm)
		S	W–H			
No. 1	$LaCoO_3$	39	50	–	–	–
No. 2	$LaCoO_3$	44	52	6	0.02	14.16
No. 3	$LaMnO_3$	22	30	–	–	–
No. 4	$LaMnO_3$	26	38	7	0.02	14.02
No. 5	$SrCoO_3$	36	51	5	0.01	7.45
No. 6	$SrMnO_3$	43	56	5	0.01	9.38
No. 7	CeO_2	46	59	–	–	–
No. 8	CeO_2	46	58	–	–	–
Nos. 9 and 10	CeO_2	51	63	–	–	–

Calculations were done using Scherrer (S) and Williamson–Hall (W–H) equations

has not yet been demonstrated [17–19]. In general, the stability of perovskites is often studied in term of the "tolerance factor", *t*-value:

$$t = \frac{r_A + r_X}{\sqrt{2}(r_B + r_X)}, \quad (3)$$

where r_A, r_B and r_X are the ionic radii of cations *A*, *B* and anion *X*, respectively. The *t*-value of the ideal perovskite should be equal to 1.0 [13, 20]. However, as an experimental fact, *t*-values of most cubic perovskites are in the range of 0.8–0.9. Distorted perovskites occur in somewhere wider range of *t*-values [13]. Tolerance factor has been widely accepted as a criterion for the formation of the perovskite structure. However, up to now, it seems that *t*-values do not provide the sufficient condition for the formation of the cubic perovskite structure [13]. Octahedral factor, r_B/r_X, is also an important factor governing formability of cubic perovskites. For a cubic perovskite structure the value of the octahedral factor should be varied with the limited range of 0.414–0.732 [13]. As seen in Table 4, in agreement with the XRD analysis, among the synthesized perovskites only $LaMnO_3$ is found to have a cubic perovskite structure. From Table 4 it is also concluded that $CeMnO_3$, in case of the formation, could have a cubic structure.

Table 4 Ionic radius, tolerance factor, and octahedral factor of the samples

Sample	*A* cation	r_A (nm)	*B* cation	r_B (nm)	*t*-value	Octahedral factor
No. 1 and 2	La^{3+}	0.103	Co^{3+}	0.055	0.88	0.39
No. 3 and 4	La^{3+}	0.103	Mn^{3+}	0.065	0.84	0.46
No. 5	Sr^{2+}	0.118	Co^{4+}	0.053	0.95	0.38
No. 6	Sr^{2+}	0.118	Mn^{4+}	0.053	0.95	0.38
No. 7	Ce^{3+}	0.101	Co^{3+}	0.055	0.87	0.39
No. 8	Ce^{3+}	0.101	Mn^{3+}	0.065	0.83	0.46

Oxide anion radius is equal to 0.140 nm [20]

It was observed that a higher calcination temperature of 900 °C is needed for the formation of Sr(Mn or Co)O_3 perovskite phases. Hence, in an effort to obtain a perovskite with cerium as the cation of site *A*, the sample No. 8 was calcined at higher temperature of 1,100 °C in air atmosphere for 5 h. Results of XRD analysis, however, show no existence of diffraction peaks of the $CeMnO_3$ (sample No. 9 in Fig. 1c). The calcination under reducing atmosphere (6 vol% CO in Ar) is not also carried out to the formation of cerium manganite (see Table 1 and sample No. 10 in Fig. 1c). The only result of the calcination at 1,100 °C under CO atmosphere is the reduction of the manganese oxide phase, i.e., Mn_2O_3 is turned to MnO phase.

FTIR results of the samples that are reported in Table 1 are shown in Fig. 2. A broad absorption band at 630 cm^{-1} in $LaMnO_3$ samples is attributed to Mn–O vibrations of MnO_6 octahedral in cubic perovskite structure [1]. The Mn–O vibrations in the case of $SrMnO_3$ appeared at 520 cm^{-1}. The widening of the *B*–O band and/or the appearance of a shoulder was reported to be an indication of a structure with lower symmetry [10]. A shoulder in the $LaCoO_3$ perovskite at 556 cm^{-1} was cited to be a characteristic of a rhombohedral structure. The absorption peak at 1,386 cm^{-1} was assigned to the asymmetrical lengthening of O–C–O vibration [5]. The absorption bands at 568 and 674 cm^{-1} are characteristic for CeO_2, as reported in literature [21]. In agreement with the XRD analysis, results

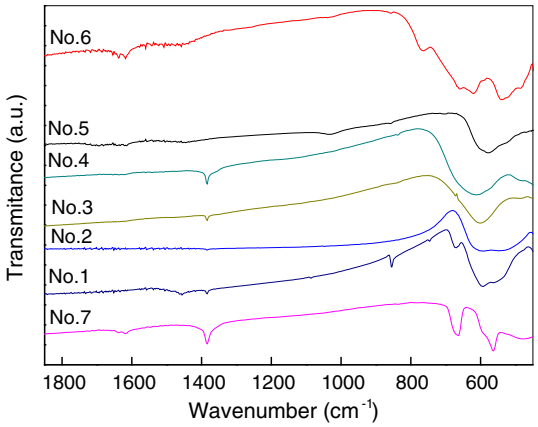

Fig. 2 FTIR spectrum of the synthesized samples nos. 1–7

of FTIR also confirmed the formation of CeO_2 instead of a perovskite phase.

The SEM micrographs of the fresh samples (Nos. 1–6) are presented in Fig. 3. The presence of citric acid prevents agglomeration of the particles to a large extent [10]. It is expected that large amount of gases is evolved during calcination at high temperatures when citric acid decomposes. The gas evaporation, however, has more effect on the porosity of $LaCoO_3$ and $LaMnO_3$ perovskites than $SrCoO_3$ and $SrMnO_3$ samples (Table 3 and Fig. 3). According to Fig. 3, it can be concluded that the increase in the calcination temperature from 600 to 900 °C does not cause the particle size increasing of $LaCoO_3$ and $LaMnO_3$ nanoparticles. The XRD results, however, show that the crystallite size of the particles is increased, which can be related to the agglomeration of crystallites.

TEM micrographs and particle size distribution of samples Nos. 1 and 3 are shown in Fig. 4. The average particle size was calculated to be 46 nm for $LaCoO_3$ and 28 nm for $LaMnO_3$, respectively. The results are somewhat different from the calculated crystallite sizes from XRD line profile. The differences are related to the irregular shape of the nanoparticles with spherical, spherodial, and polygon morphologies which are observed by TEM [1].

The particle size distribution (PSD) of samples Nos. 1 and 3, obtained by cumulant method, are presented in Fig. 4c, f. Results are related to a dispersed sample in ethanol. A mean diameter of $\sim$26 and $\sim$20 nm is measured for particles of samples Nos. 1 and 3, respectively. Thus, the prepared samples are entirely within the nanoscale domain. The particle size, obtained from particle size analyzer, has been almost correlated with the measurements of particle size from XRD and TEM analyses. Results of PSD also indicate that for $LaMnO_3$ and $LaCoO_3$ nanoparticles the highest percentage is around 12 and 23 nm, respectively. As can be seen in Fig. 4, sample No. 1 ($LaCoO_3$) has a more symmetric distribution than sample No. 3 ($LaMnO_3$).

Catalytic performance tests of La(Mn or Co)O_3 and Sr(Mn or Co)O_3 perovskites for carbon monoxide oxidation are shown in Table 5. The catalytic activity of the perovskite samples chiefly depends on three factors: chemical composition, degree of crystallinity and morphology (including particle size, pore size distribution, and specific surface). The temperature corresponding to 50%

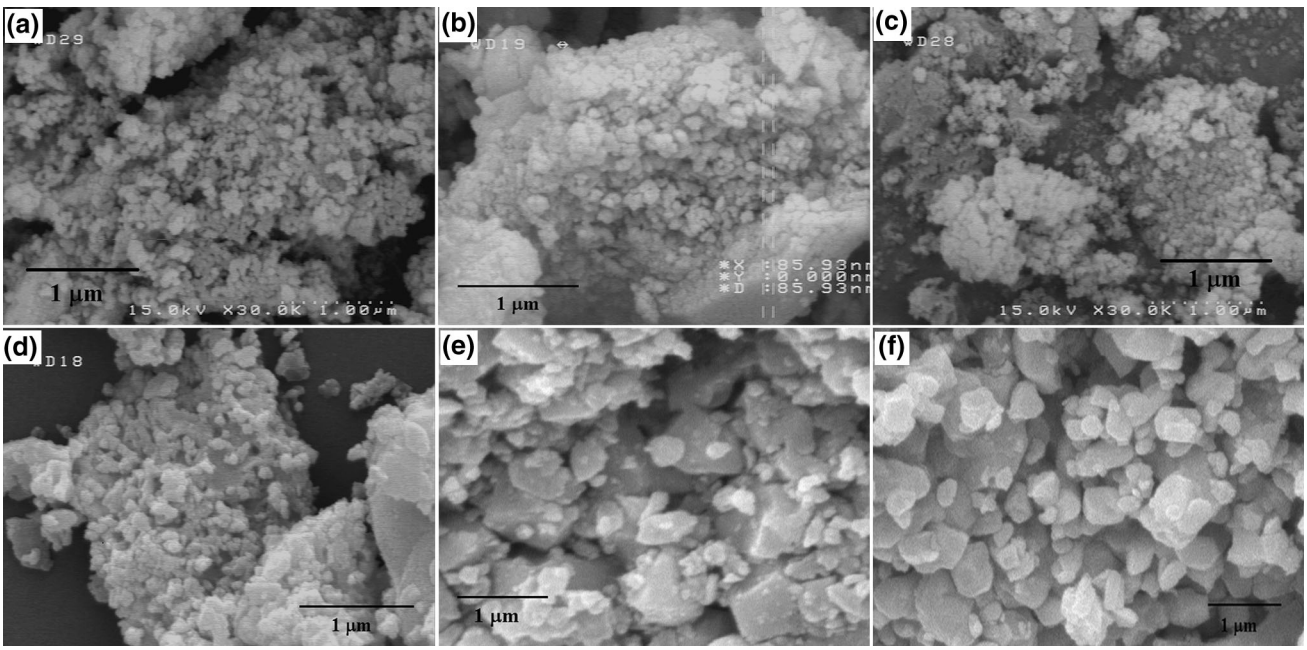

Fig. 3 SEM micrographs of the samples: No. 1 **a**, No. 2 **b**, No. 3 **c**, No. 4 **d**, No. 5 **e**, No. 6 **f**

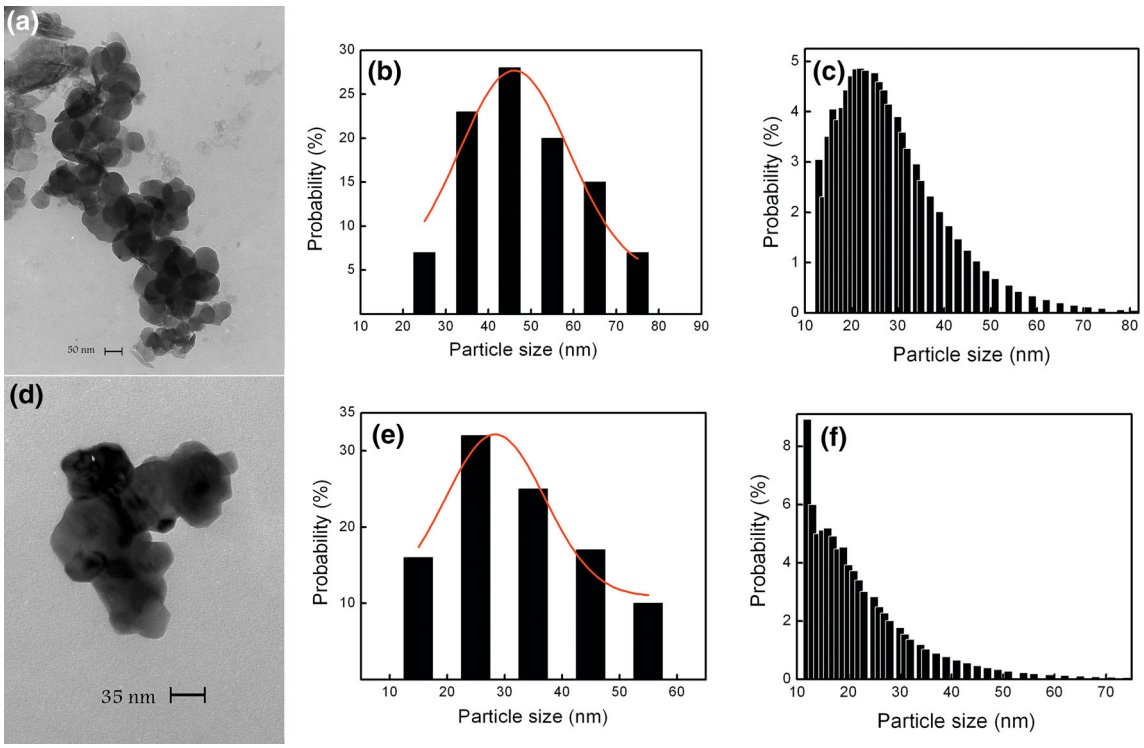

Fig. 4 TEM micrographs **a**, **d**, size distribution histograms obtained from TEM analysis **b**, **e** and particle size distribution histograms obtained from particle size analyzer **c**, **f** for the samples: No. 1 **a–c**, No. 3 **d–f**

Table 5 CO oxidation temperature (°C) according to the CO conversion fraction for the prepared samples

Sample	10%	50%	90%
No. 1	116	183	199
No. 2	192	215	232
No. 3	145	154	162
No. 4	145	212	228
No. 5	265	295	338
No. 6	215	285	333

conversion of CO is defined as the catalyst light off temperature and is an important parameter in catalytic reactions. The lower the light off temperature, the more active the catalyst is. According to the reaction temperature, the $LaMnO_3$ sample is the best catalyst for the CO oxidation. This can be attributed to the higher BET surface area and smaller particle size of the $LaMnO_3$ perovskite (Table 3). Increasing the calcination temperature from 600 to 900 °C has a destructive effect on the catalytic performance of the $LaMnO_3$ and $LaCoO_3$ perovskites. According to the XRD and SEM results, this can be related to the agglomeration of crystallites which occurs at high temperatures and as a result decreases the surface area and catalytic performance. Smaller crystallite size is observed for $SrCoO_3$ in comparison with the $LaCoO_3$ perovskite (Table 3). A better catalytic activity, however, is observed over $LaCoO_3$ sample (Table 5). This can be related to the higher BET of $LaCoO_3$ which confirms less agglomeration of this sample in contrast with $SrCoO_3$ nano-perovskite.

4 Conclusion

The structural and catalytic properties of (Ce, La, or Sr)(Mn or Co)O_3 samples for CO oxidation were investigated. Citric acid is a proper additive that decreases particle size of the prepared nano-particles. Cerium oxide showed more stability in comparison with $CeCoO_3$ and $CeMnO_3$ nano-perovskites, and was the predominant crystalline phase in course of the preparation of cerium cobaltite or cerium manganite. Finding of a proper method for the preparation of these nanoperovskites is under research to obtain a better catalyst for the CO oxidation in comparison with the La(Mn or Co)O_3 nanoperovskites.

References

[1] E. Frozandeh-Mehr, A. Malekzadeh, M. Ghiasi, A. Gholizadeh, Y. Mortazavi, A. Khodadadi, Catal. Commun. **28**, 32 (2012)
[2] S. Sartipi, A.A. Khodadadi, Y. Mortazavi, Appl. Catal. B Environ. **83**, 214 (2008)

[3] A. Civera, M. Pavese, G. Saracco, V. Specchia, Catal. Today **83**, 199 (2003)
[4] P. Femina, P. Sanjay, Res. J. Recent Sci. **1**, 178 (2012)
[5] M. Ghiasi, A. Malekzadeh, Cryst. Res. Technol. **47**, 471 (2012)
[6] R.G. Shetkar, A.V. Salker, J. Mater. Sci. Technol. **26**, 1098 (2010)
[7] R. Zhang, H. Alamdari, S. Kaliaguine, J. Catal. **242**, 241 (2006)
[8] K.C. Patil, S.T. Aruna, T. Mimani, Curr. Opin. Solid State Mater. Sci. **6**, 507 (2002)
[9] A. Chakroborty, A.D. Sharma, B. Maiti, H.S. Maiti, Mater. Lett. **57**, 862 (2002)
[10] M. Khazaei, A. Malekzadeh, F. Amini, Y. Mortazavi, A. Khodadadi, Cryst. Res. Technol. **45**, 1064 (2010)
[11] K. Umemoto, Y. Seto, Y. Masuda, Thermochim. Acta **431**, 117 (2005)
[12] Z. Yang, L. Ye, X. Xie, Phys. Rev. B **59**, 7051 (1999)
[13] L.M. Feng, L.Q. Jiang, M. Zhu, H.B. Liu, X. Zhou, C.H. Li, J. Phys. Chem. Solids **69**, 967 (2008)
[14] P. Kameli, H. Salamati, A. Aezami, J. Appl. Phys. **100**, 53914 (2006)
[15] I. Atribak, A. Bueno-Lopez, A. Garcia-Garcia, Catal. Commun. **9**, 250 (2008)
[16] D.H. Lee, J.S. Park, C.H. Yo, K.H. Kim, Mater. Chem. Phys. **40**, 184 (1995)
[17] W. Wunderlich, H. Fujiwara, J. Electron. Mater. **40**, 127 (2011)
[18] K. Umemoto, Y. Seto, Y. Masuda, Thermochim. Acta **431**, 117 (2005)
[19] Y. Shao, X.F. Wang, M. Ao, C.R. Gong, G.L. Fan, H.F. Chen, Front. Mater. Sci. **6**, 304 (2012)
[20] L.Q. Jiang, J.K. Guo, H.B. Liu, M. Zhu, X. Zhou, P. Wu, C.H. Li, J. Phys. Chem. Solids **67**, 1531 (2006)
[21] L. Pautrot, P. Barboux, J.P. Biolot, J. Sol–Gel. Sci. Technol. **39**, 261 (2006)